

There is no $\kappa(900)$

S. N. Cherry and M. R. Pennington

*Centre for Particle Theory,
University of Durham,
Durham DH1 3LE, U.K.*

Abstract

In the $I = 0$ sector there are more scalar mesons than can fit in one $q\bar{q}$ nonet. Consequently, many have claimed that there is in fact more than one multiplet, perhaps both $q\bar{q}$ and $qq\bar{q}\bar{q}$. Such proposals require the existence of at least two strange isodoublets (and their antiparticles). The current PDG Tables list just one state, the $K_0^*(1430)$, while fits to data with Breit-Wigner forms and variable backgrounds can accommodate a $\kappa(900)$ too. Whether a state exists in the spectrum of hadrons is not a matter of ability to fit data along the real energy axis, but is completely specified by the number of poles in the complex energy plane. Here we perform as model-independent an analytic continuation of the LASS πK scattering results between 825 MeV and 2 GeV as presently possible to determine the number and position of resonance poles. We find that there **is** a $K_0^*(1430)$, but **no** $\kappa(900)$. The LASS data cannot rule out the possibility of a very low mass κ well below 825 MeV.

PACS numbers: 11.55.-m, 14.40.Ev

Keywords: Analytic Properties, Scalar Mesons, Strange Mesons.

1 Introduction

For many years the scalar mesons have caused controversy. There is little consensus on the composition of many states, whilst for some their properties and even existence is a matter for debate. In the latest edition of the PDG Tables [1], there are four scalar-isoscalars below

1.55 GeV, with a fifth at 1.7 GeV. This is obviously too many for a standard $q\bar{q}$ nonet. However, many QCD-motivated models predict the existence of non- $q\bar{q}$ mesons, such as $qq\bar{q}\bar{q}$ states [2], $K\bar{K}$ molecules [3] and glueballs [4], and it is precisely in the isoscalar sector that these unconventional mesons are most likely to be found. This excess of isoscalars, together with the existence of two isovectors, the $a_0(980)$ and $a_0(1450)$, has been suggested as evidence for two scalar nonets [5, 6]: the conventional $q\bar{q}$ nonet lying around 1.4 GeV with an unconventional one centred around 1 GeV. However, the PDG lists only one pair of scalar-isospinors in this mass region, the $K_0^*(1430)$. This has led some authors to postulate a light strange meson, known as the κ [2, 7, 8]. Evidence for this resonance has been claimed within certain models [9, 10, 11, 12], whilst other studies dispute this [13, 14]. Fits to πK production data, using Breit-Wigner forms, some with arbitrarily varied backgrounds, others with theoretically motivated backgrounds, allow a κ to be accommodated. However, the existence of a state is not a matter merely of the quality of fit to data along the real energy axis. Indeed, a state is wholly specified by there being a pole of the S -matrix in the complex energy plane on the nearby unphysical sheet. Such specification, of course, does require experimental information in the relevant region of the real energy axis.

Where this light strange meson has a mass around 900 MeV, it comes within the energy domain testable with the highest statistics results on πK scattering, which come from the LASS experiment [15]. In this paper we present the results of a close to model independent determination of the number and position of poles in the $I = \frac{1}{2}$, $J = 0$ πK scattering amplitude based on these LASS data above 825 MeV. The technique relies wholly on the analytic properties of S -matrix elements and requires no artificial separation into resonance and background contributions. We also consider continuations using results from an earlier SLAC experiment [16]. In Sect. 2, we present the method and then in Sect. 3 describe the experimental inputs we use. In Sect. 4, we apply the analytic continuation methodology first to model data to assess its capabilities and limitations. In Sect. 5, we go on to study the analytic continuation using the real experimental results. We find there is no $\kappa(900)$. Since the method is one of continuing experimental data and the LASS experiment only provides information above 825 MeV we cannot rule out the possibility of an even lower mass κ . In Sect. 6, we conclude.

2 Method

The method we use is due to Nogová *et al.* [17]. It combines simple statistics with the analytic properties of the scattering amplitude to locate the positions of poles. As usual, we expect resonances to correspond to poles on unphysical sheets [18].

2.1 Mapping

In order to locate poles in the complex plane from scattering data on partial wave amplitudes along the real axis, we must perform an analytic continuation. To maximise the domain in which this continuation is valid, we begin by conformally mapping the partial wave amplitude into the unit disc. As shown in Fig. 1, for πK scattering the s -plane is split into two regions and in this case we map the region *outside* the circular cut. The mapping is designed so that the cuts of the partial wave amplitude in the s -plane are mapped onto the circumference of the circle in the z -plane. This allows us to continue the amplitude throughout the complex z -plane.

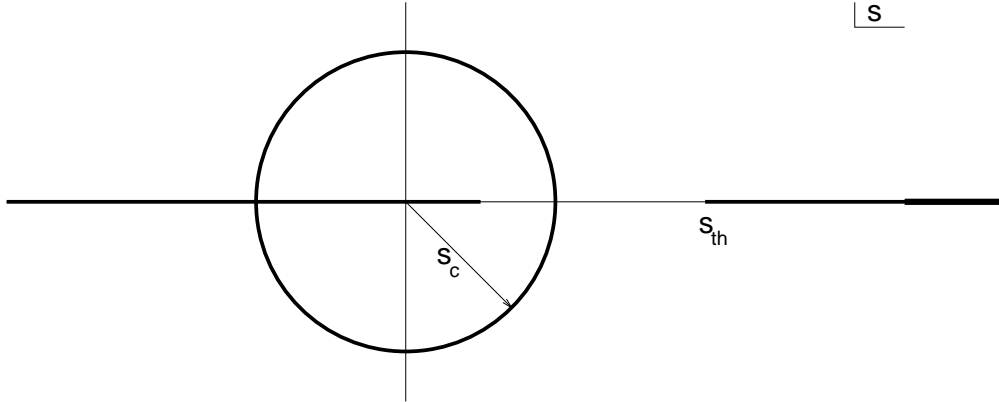


Figure 1: The cut structure of the πK partial wave amplitude, where $s_{th} = (m_K + m_\pi)^2$ and the radius of the circular cut is $s_c = m_K^2 - m_\pi^2$.

The mapping is accomplished in two steps. Firstly,

$$y(s) = \left(\frac{s - s_c}{s + s_c} \right)^2, \quad (1)$$

which maps the real cuts in the s -plane onto the positive real axis of the y -plane and the circular cut onto the negative real axis. Then to map the twice cut y -plane into the unit disc, we define

$$z(s) = \frac{i\beta\sqrt{y(s)} - \sqrt{y(s) - y(s_{th})}}{i\beta\sqrt{y(s)} + \sqrt{y(s) - y(s_{th})}} \quad , \quad (2)$$

where β is a real parameter which is chosen so that the region of interest in the s -plane is mapped close to the imaginary axis in the z -plane, thereby minimising the distance the continuation must cover. The points $s = s_{th}$ and $s = s_c$ are fixed for any value of β , being mapped to $z = 1$ and $z = -1$ respectively. Notice that the cuts in the upper half of the s -plane (such as the region where physical data lie) are mapped to the upper semi-circle in Fig. 2.

It is obvious from this mapping that the physical region in the s -plane only covers a fraction of the circle. Even if we had data over an infinite range of energies, we could never complete the circle, see Fig. 2. Nevertheless, we only need analytically continue very close to the region of data (i.e. the solid arc in Fig. 2). We shall return to this point later.

From Fig. 2 we can see that the mapping is highly non-linear in the following sense. As we increase the energy from threshold to infinity, the proportion of the circle covered by each increment falls very sharply. It is clear that the region between threshold (at 633 MeV) and the start of the data (at 825 MeV) covers a much longer arc than the region in which we have data (825 MeV to 2.51 GeV) and the region between the end of the data and infinite energy is much smaller still. This compression of the high energy region would suggest that the method is less sensitive to higher mass resonances. This apparent weakness actually has some benefit. As we explain in the next section, we test the scattering amplitude against the hypothesis that it contains a given number of poles. The computational burden increases rapidly as we increase the number of poles, so if we had to account for all the possible radial excitations in a given channel the calculation would soon become computationally prohibitive. Consequently, the procedure is only practicable for the lowest few states.

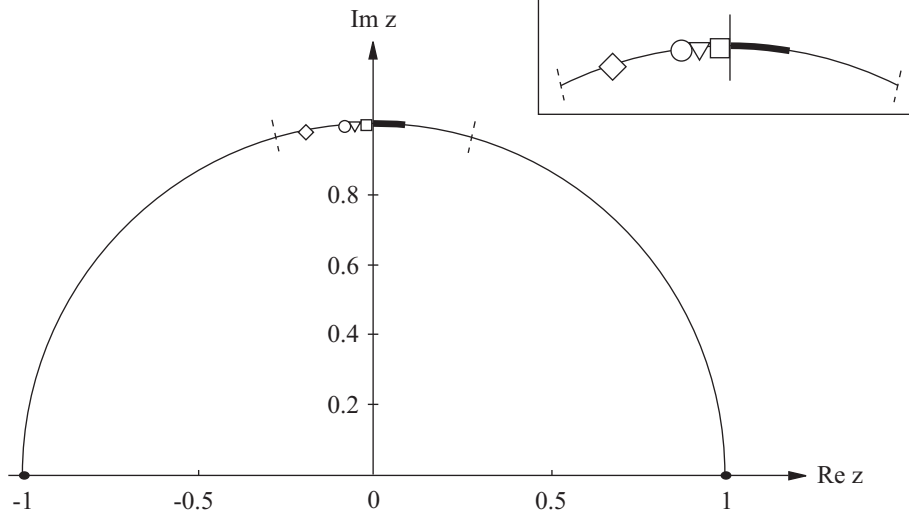


Figure 2: The z -plane showing how points in s -plane map. The mapping parameter β is chosen so that $s = (1.4 + 0.15i)^2 \text{ GeV}^2$ is mapped to the imaginary axis. The thicker line shows the arc covered by the LASS data. The inset shows an enlargement of the key region close to $z = i$, from where we analytically continue. The symbols mark particular values of s as follows: $\blacklozenge s = s_{th}$, $\square s = \infty$, $\nabla s = -s_c$, $\circ s = is_c$, $\diamond s = \frac{1}{\sqrt{2}}(s_c + is_c)$, $\bullet s = s_c$.

2.2 Analytic Continuation

For now we assume that we have a scattering amplitude, with errors, Δ_i ,¹, defined at discrete points all the way around our circle $|z| = 1$. We define $|\delta z_i|$ as the average distance between the i th data point and its two nearest neighbours in the complex z -plane shown in Fig. 2. In regions where these discrete points are densely packed, our scattering amplitude is most tightly controlled and so we weight the error on each point by the density of the data points in that region, $\epsilon_i(z) = \Delta_i \sqrt{|\delta z_i|/2\pi}$. We make a smooth interpolation to the amplitude, $Y(z)$, and the weighted errors, $\epsilon(z)$, so that we have continuous functions defined on the entire circle. This weighting procedure ensures that the small region of the unit circle in Fig. 2, where we have experimental data, controls the analytic continuation into the nearby region where resonance poles are expected to sit. If $F(z)$ is a square integrable function on the circle, C , then we can test how well this function describes the data through a χ^2 ,

¹This method requires the errors on the real and imaginary parts of the amplitude to be equal. This simplification is arranged by taking the value of the error to be the larger of the error on the real part and the error on the imaginary part at any given energy.

defined by

$$\chi^2 = \frac{1}{2\pi} \oint_C \left| \frac{F(z) - Y(z)}{\epsilon(z)} \right|^2 |dz| \quad . \quad (3)$$

We now introduce a non-zero weight function $g(z)$, which is defined to be real analytic and constrained by $|g(z)| = \epsilon(z)$ around the circle. We expand the data and the trial function as Laurent series about the origin, so that

$$y(z) = \frac{Y(z)}{g(z)} = \sum_{k=-\infty}^{\infty} y_k z^k \quad , \quad f(z) = \frac{F(z)}{g(z)} = \sum_{k=-\infty}^{\infty} a_k z^k \quad . \quad (4)$$

Since partial wave amplitudes are real analytic, the coefficients a_k and y_k are real. Although we are expanding about the origin, the expansion is carried out round the circle, since this is where we have data. The singular Laurent coefficients will pick up any poles within the disc. Substituting Eq. (4) into Eq. (3) gives

$$\chi^2 = \sum_{k=1}^{\infty} (a_{-k} - y_{-k})^2 + \sum_{k=0}^{\infty} (a_k - y_k)^2 \quad . \quad (5)$$

The pole structure of our partial wave amplitude, $Y(z)$, can then be determined by finding the test function $F(z)$ which minimises the first summation in Eq. (5).

If we want to test against the assumption that there are no poles in the data we must use a test function that is analytic, i.e. $a_{-k} \equiv 0$ for $k > 0$. Then, if the amplitude has no poles, the quantity $\chi_0^2 = \sum_{k=1}^N y_{-k}^2$ will be zero². If we think that the scattering data has one pair of complex conjugate poles in the z -plane (as is the case where there is one resonance present) then we can write our test function as

$$\begin{aligned} f(z) &= \frac{\alpha}{z - z_0} + \frac{\alpha^*}{z - z_0^*} + h(z) \\ &= \sum_{k=1}^{\infty} \frac{2 \Re[\alpha z_0^{k-1}]}{z^k} + h(z) \quad , \end{aligned} \quad (6)$$

where $h(z)$ is some analytic function. By comparing Eq. (6) with Eq. (4) we see that, in this case, the analytic continuation is carried out by setting $a_{-k} = 2 \Re[\alpha z_0^{k-1}]$ and then it is the quantity $\chi_1^2 = \sum_{k=1}^N (y_{-k} - 2 \Re[\alpha z_0^{k-1}])^2$ that has a χ^2 distribution with N degrees of freedom as long as $|z_0| \ll 1$.

²Actually, due to inevitable experimental noise, χ_0^2 will not be exactly zero, but should fit a χ^2 distribution with N degrees of freedom.

However, in practice $|z_0|$ is close to one and the above procedure becomes unreliable. Consequently, we adopt the alternative approach of cancelling any pole in the data explicitly by the introduction of the so-called Blaschke pole-killing factor. This avoids the need to make the expansion explicit in Eq. (6) and so significantly improves the convergence. For a pair of complex conjugate poles the Blaschke factor looks like

$$B_{z_0} = \frac{(z - z_0)(z - z_0^*)}{(1 - z z_0)(1 - z z_0^*)} \quad . \quad (7)$$

We define the function

$$\tilde{y}(z) = \frac{Y(z)B_{z_0}(z)}{g(z)} = \sum_{k=-\infty}^{\infty} \tilde{y}_k z^k \quad (8)$$

and then the quantity $\sum_{k=1}^N (\tilde{y}_{-k})^2$ will indeed obey a χ^2 distribution with N degrees of freedom, if the actual amplitude contains one pair of complex conjugate poles.

3 Experimental Input

Our experimental information on the S -wave πK partial wave amplitude comes in the form of the magnitudes, $a(s)$, and phases, $\phi(s)$, measured, for instance, by the LASS experiment. The partial wave amplitude on sheet I is normalised thus

$$f^I(s) = \frac{a(s) e^{i\phi(s)}}{\rho(s)} \quad , \quad (9)$$

where $\rho(s) = 2q/\sqrt{s}$ and q , the c.m. 3-momentum

$$q = \frac{1}{2} \sqrt{\frac{[s - (m_K + m_\pi)^2][s - (m_K - m_\pi)^2]}{s}} \quad . \quad (10)$$

πK scattering has two possible isospin channels, $I = 1/2$ and $I = 3/2$. The resonances we consider are isodoublets, as there are no known resonances in the $I = 3/2$ channel. This means that there is no need to separate the isospin components to determine the pole positions, whereas this is essential in a Breit-Wigner-type fit. We therefore carry out our analysis for the total S -wave data. However, as a check we also perform this for the $I = 1/2$ results alone. Of course, the $I = 1/2$ data must be extracted from the total S -wave data by subtracting an assumed form for the $I = 3/2$ amplitude, thereby introducing an additional

layer of uncertainty. Moreover, this separation is only possible over a limited energy range. Nevertheless, the $I = 1/2$ component does provide a valuable check.

As is well-known, resonance poles do not appear on the physical sheet in the energy plane. Consequently, we must move to the relevant unphysical sheet. For purely elastic scattering this would be sheet II. In practice for πK scattering, the ηK channel opens very weakly (in agreement with $SU(3)_F$ expectations) and so any inelasticity can be safely neglected, until one reaches the $\eta' K$ threshold. This channel opens in the region of a possible $K_0^*(1430)$ and complicates the sheet structure. Any resonance would then be on sheet III³. We must take this threshold into account when we change sheets. The simplest way to pick the correct sheet is to change the sign of the phase, i.e.

$$f^{II}(s) = \frac{a(s) e^{-i\phi(s)}}{\rho(s)} \quad . \quad (11)$$

This moves us onto sheet II below the $\eta' K$ threshold and sheet III above it. This method of changing sheets is also valid for the total S -wave amplitude. We then map the data, including errors, as described above.

As noted previously it is not possible to cover the circle completely with physical region data, since we do not have experimental results either close to threshold or on the circular and left hand cuts (see Fig. 1). The exact proportion of the circle covered by the direct channel πK results depends on the choice of the mapping parameter β . How we treat the near threshold arc of Fig. 2 is a little different for our model tests of Sect. 4 and when we consider the actual experimental data in Sect. 5. Consequently, we detail their treatment in the appropriate section. As we do not have information about what happens on the unphysical cuts, we simply make a guess. So that the guess does not unduly affect the results, we de-weight these guessed points by giving them very large errors and by ensuring that they are widely spaced (see Fig. 3). With the top semi-circle now spanned by data points, we make an interpolation to give us a continuous function. We complete the circle by reflecting the interpolated data in the upper semi-circle onto the lower half so as to obey the Schwarz Reflection Principle.

A suitable form for the weight function $g(z)$, which fulfills all the conditions described

³The Riemann sheets are labelled by (r_1, r_2) , where the r_j are the signs of the imaginary parts of the complex phase spaces ρ_j in particular channels. $j = 1$ for πK , $j = 2$ for $\eta' K$. Sheet I is $(+, +)$, sheet II is $(-, +)$ and sheet III is $(-, -)$

above is

$$g(z) = \exp \left(\sum_{n=0}^N c_n z^n \right) \quad (12)$$

where the c_n are found from a Fourier cosine fit to $\ln \epsilon(z)$. We take $N = 100$. The singular coefficients of the Laurent expansion of the data about the origin are just

$$y_{-k} = \frac{1}{2\pi} \oint_c \frac{Y(z) z^k}{g(z)} |dz| \quad . \quad (13)$$

4 Results from Model Data

As a first application, the method described in Sect. 3 is tested on a model amplitude describing the situation where a light, broad resonance, κ_1 , and a heavier, narrower resonance, κ_2 , are present⁴. The resonances are constructed using Jost functions, with the lighter, broader resonance being treated as the background at the second resonance, *i.e.*

$$f^I(s) = f_1^I(s) + e^{2i\delta_1(s)} f_2^I(s) \quad (14)$$

on the first sheet, where

$$f_j^I(s) = \frac{-2kd_j}{\rho(k + c_j + id_j)(k - c_j + id_j)} \quad , \quad (15)$$

$$\delta_1(s) = \arctan \left(\frac{2kd_1}{c_1^2 + d_1^2 - k^2} \right) \quad , \quad (16)$$

$$k = \frac{1}{2} \sqrt{s - (m_K + m_\pi)^2} \quad . \quad (17)$$

The four parameters $\{c_j, d_j\}$ are chosen, so that the amplitude has poles at $s_1 = (0.9 \pm 0.25i)^2 \text{ (GeV)}^2$ and $s_2 = (1.4 \pm 0.15i)^2 \text{ (GeV)}^2$. Data are created for energies equivalent to the full LASS data-set [15], with the error on both the magnitude and phase fixed at 5%. Below the energy of the LASS data, we create a few equally spaced points between threshold and 825 MeV. This will be discussed in more detail later. The amplitude in the unphysical region is set to a real constant (incidentally equal to the amplitude at threshold) with very large errors (± 5). These model data are illustrated in Fig. 3.

⁴This generalises a model analysis discussed by Nogová *et al.* to two resonances.

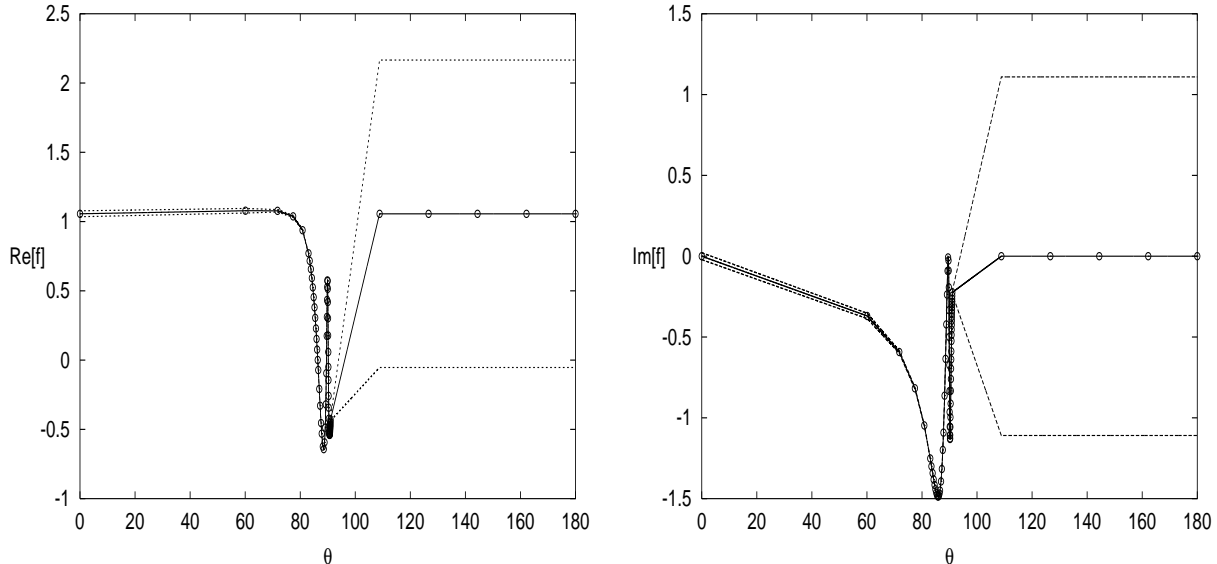


Figure 3: Real and imaginary parts of f^{II} as a function of θ , the angular position around the circle in degrees, for the model data-set. The circles represent data points, the solid line shows the interpolation to the data and the dashed line shows the interpolated weighted errors.

These model data allowed us to verify that the Blaschke factor method is indeed more stable to variations of non-physical parameters (such as the number of terms in our definitions of the χ^2 and the weight function) and hence more accurate. The pole positions and χ^2 's found by fitting over the first 40 singular coefficients using this procedure are shown in Table 1. Also tabulated for comparison are the results obtained when the errors on the points in the unphysical region are halved.

From Table 1, it is clear that the method is readily capable of identifying the number and position of poles even when the associated resonances are broad and overlapping. The decrease in χ^2 when going from no resonance to one resonance is large, but far less significant than the fall when we ask is there one or two resonances. From this Table, one would have no doubt that there are two resonances in the model data and their positions are well determined.

Evaluating the errors on the pole positions that we obtain using this method is nevertheless not straightforward. The experimental errors are folded into the actual calculation and so their propagation cannot easily be followed. Moreover, as pointed out by Nogová *et al.* [17], the χ^2 's obtained are not strictly statistical, so the standard confidence level techniques are not appropriate. Thus we resort to an order of magnitude estimate of the

Option	No. of resonances	z_{pole} (r, θ)	$\sqrt{s_{pole}}$ (MeV)	χ^2
1	0	—	—	4081
	1	(0.988, 89.31°)	$1201 \pm 131i$	281
	2	(0.993, 89.98°) (0.943, 88.64°)	$1396 \pm 142i$ $903 \pm 234i$	0.5
2	0	—	—	3759
	1	(0.989, 89.13°)	$1173 \pm 111i$	417
	2	(0.993, 89.97°) (0.942, 88.61°)	$1392 \pm 140i$ $900 \pm 233i$	1.0

Table 1: Pole positions and χ^2 's for model data. Option 1 has the unphysical errors set to 5. Option 2 has the unphysical errors set to 2.5.

errors obtained by varying the inputs that introduce uncertainty into the calculation. These inputs include the number of terms in the Fourier expansion defining the weight function, the number of terms in the summation used to evaluate χ^2 and the treatment of the unphysical region. The uncertainty in the pole position found in the z -plane due to these changes in parameters is shown in Fig. 4, from which we see that the typical uncertainty in the z -plane is of the order of $(4 + 20i) \times 10^{-5}$.

Max. Energy	χ_0^2	χ_1^2	χ_2^2	λ (MeV)	λ_1 (MeV)	λ_2 (MeV)
22.51	2320	43.3	2.02	$1395 \pm 53i$	$1938 \pm 234i$	$1453 \pm 137i$
12.51	2361	37.0	1.98	$1394 \pm 56i$	$1951 \pm 253i$	$1456 \pm 133i$
8.51	2389	35.0	1.96	$1394 \pm 58i$	$1959 \pm 264i$	$1457 \pm 130i$
6.51	2380	18.9	1.84	$1395 \pm 69i$	$2024 \pm 331i$	$1458 \pm 114i$
3.51	2207	11.4	1.77	$1396 \pm 78i$	$2099 \pm 441i$	$1454 \pm 102i$
2.91	1959	7.33	1.70	$1398 \pm 84i$	$2178 \pm 788i$	$1445 \pm 91i$
2.51	1529	4.58	1.57	$1399 \pm 92i$	$899 \pm 1457i$	$1422 \pm 82i$

Table 2: χ^2 's and pole positions for trial data described in the text. Maximum energies are in GeV. λ is the pole position found when searching for one resonance. λ_1 and λ_2 are the pole positions found when searching for two resonances. χ_0^2 , χ_1^2 , and χ_2^2 are the χ^2 's assuming no, one and two resonances respectively. The actual pole positions are $(1421 \pm 119i)$ MeV for the κ_2 and $(1957 \pm 106i)$ MeV for the κ_3 .

Of course the physical amplitude will contain many resonances with masses greater than those of our κ_1 and κ_2 . As was stated earlier, this method is expected to be less sensitive to

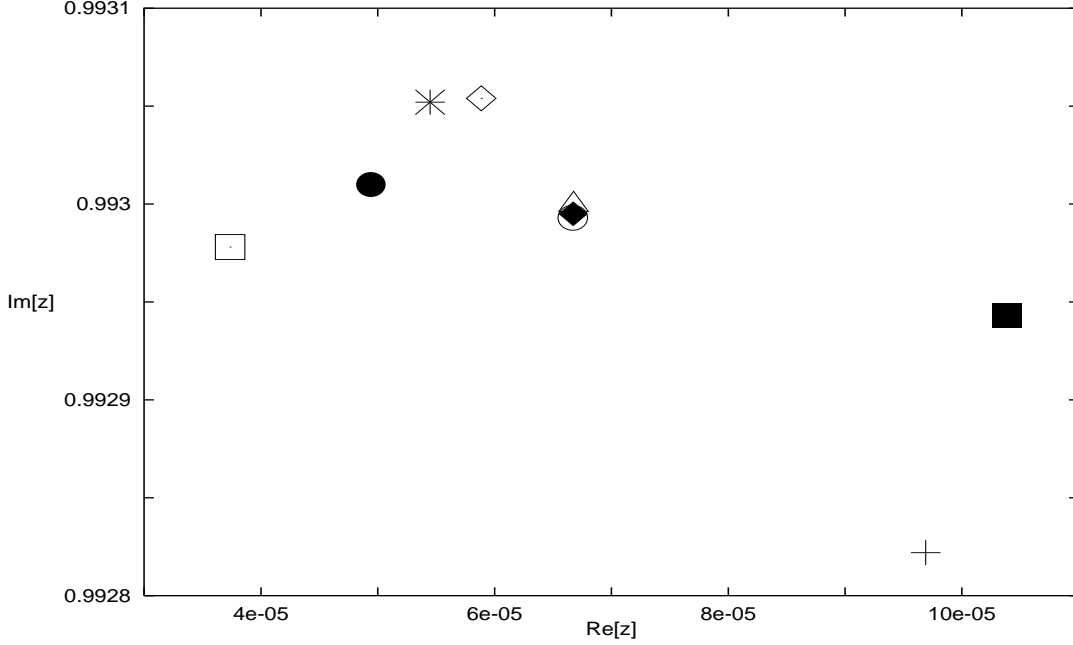


Figure 4: Expanded view of the z -plane showing the spread of pole positions found by varying the input parameters. \blacklozenge : standard values. \diamond : double the number of terms in $g(z)$. $+$: halve the number of terms in $g(z)$. $*$: Double the number of terms in χ^2 . \square : Halve the number of terms in χ^2 . \circ : Double the value of $f(z)$ in the unphysical region. \triangle : Halve the value of $f(z)$ in the unphysical region. \blacksquare : Halve the errors in the unphysical region. \bullet : Double the number of points in the unphysical region, i.e not in the direct channel.

these poles. To see to what extent this is true a further test was carried out using trial data, up to various energies, containing an effective range background, a κ_2 and another state at 1.95 GeV, which we refer to as the κ_3 . Data points were created at the same energies as the LASS data and above that at 40 MeV intervals with an error of 5%. The χ^2 's and pole positions found are shown in Table 2. From these results we can clearly see that, as the maximum energy of the data falls, the κ_3 becomes less necessary to describe the data in the z -plane. With data up to 22.5 GeV, there is a strong case for claiming that there are both the κ_2 and the κ_3 , but their parameters are not accurately found. When the data only extends to 2.5 GeV, the ratio of χ_1^2 to χ_2^2 is small enough that one would not be confident in claiming that the data exhibited more than one resonance. While the position of the κ_2 is more stable, the parameters found for the κ_3 bear no resemblance to the correct values. Meanwhile, the pole parameters found when testing for just one pole are always recognisable as the κ_2 . If we introduce realistic experimental errors and inelasticity, then the κ_3 becomes even more hidden.

Due to the non-linearity of the mapping a fixed absolute uncertainty in the z -plane will give different uncertainties in the E -plane depending on the actual position. The minimum uncertainty in the position of the κ_2 is of the order of 3 MeV on the real part and 5 MeV on the imaginary. For the κ_3 the minimum uncertainty would be 5 MeV on the real part and 15 MeV on the imaginary part. In contrast, for the κ_1 the minimum uncertainty is of the order 1 MeV on both parts. The pole positions listed in Table 1 would suggest that these minimum uncertainties underestimate the true uncertainty and we can expect to do no better than an accuracy of 10 MeV on the real part and 20 MeV on the imaginary part of the pole position.

5 Results from Real Data

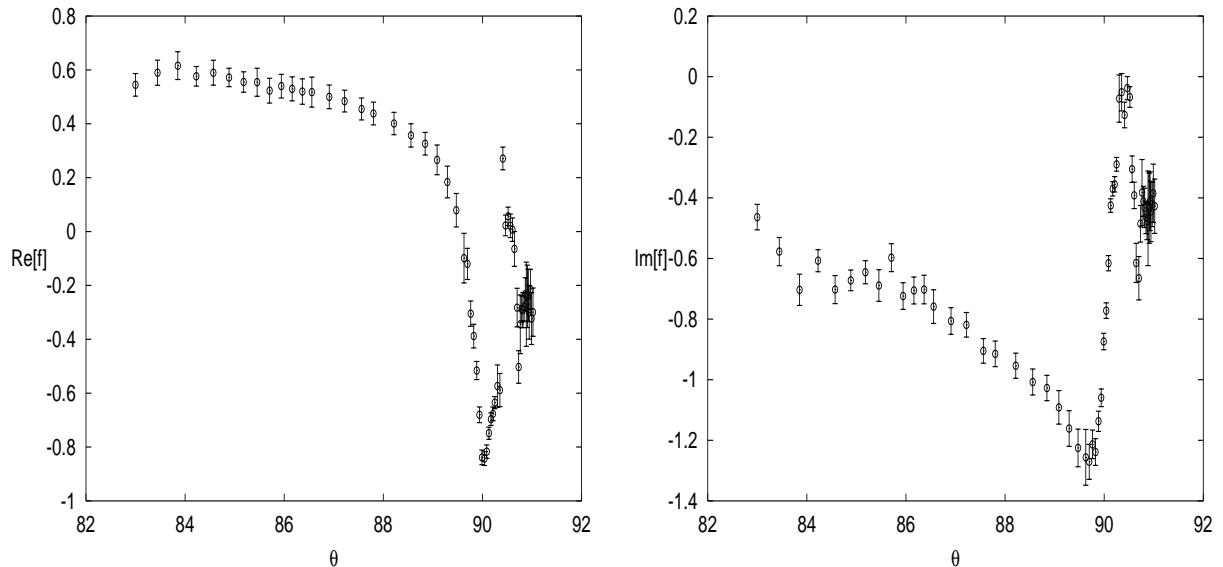


Figure 5: Real and imaginary parts of f^{II} as a function of θ for the LASS S -wave data-set. Only the actual data points are shown, with unweighted errors.

Having assessed the capabilities and limitations of the method using model data, we now apply it to the results from real experiments. From LASS [15], we have the magnitude and phase of the π^+K^- S -wave amplitude from 825 MeV up to 2.51 GeV as shown in Fig. 5. Due to a Barrelet ambiguity, the LASS group find two partial wave amplitude solutions which only differ above 1.84 GeV. For our calculation we use their Solution A, but this choice of solution does not affect our conclusions regarding the $\kappa(900)$ and the $K_0^*(1430)$.

The total S -wave amplitude for $\pi^+ K^- \rightarrow \pi^+ K^-$ is related to the amplitudes with definite isospin⁵ by

$$f_S(s) = f^{(1/2)} + \frac{1}{2} f^{(3/2)} \quad . \quad (18)$$

Since resonances are only expected in the $I = 1/2$ channel, it is natural to consider the effect of separating out this component. Such a separation requires a modelling of the $I = 3/2$ contribution. Below 1.58 GeV, the LASS group provide a model of this contribution based on the parametrisation of Estabrooks [19]. This allows us to apply the method used in Sect. 4 to the $I = 1/2$ amplitude alone, but only below 1.58 GeV. As a control on this procedure, we also consider the full S -wave data over this reduced energy range, which we refer to as the “Short S -wave data-set”.

The effective range type formula provided by LASS gives one possible extrapolation of their data to threshold. This serves as *a guide* (and only a guide) to possible data points between threshold and the start of the data. Note that the superscript (I) is an isospin label. All equations for amplitudes in this section refer to the physical sheet. Their formula is

$$f^{(I)} = \frac{1}{\rho (\cot \delta_{BG}^{(I)} - i)} + \frac{e^{2i\delta_{BG}^{(I)}}}{\rho (\cot \delta_{BW} - i)} \quad , \quad (19)$$

where the resonance term only appears in the $I = 1/2$ case and

$$q \cot \delta_{BG}^{(I)} = \frac{1}{a^{(I)}} + \frac{1}{2} b^{(I)} q^2 \quad , \quad (20)$$

$$\cot \delta_{BW} = \frac{(m_r^2 - s) E q_r}{m_r^2 \Gamma_r q} \quad . \quad (21)$$

q is given by Eq. (10), and q_r is its value at $s = m_r^2$. The LASS fit⁶ gave $a^{(1/2)} = 2.19 \text{ GeV}^{-1}$, $b^{(1/2)} = 3.74 \text{ GeV}^{-1}$, $a^{(3/2)} = -1.03 \text{ GeV}^{-1}$, $b^{(3/2)} = -0.94 \text{ GeV}^{-1}$, $m_r = 1.412 \text{ GeV}$ and $\Gamma_r = 0.294 \text{ GeV}$. It is important to recognise that though the LASS effective range fit assumes the tail of a Breit-Wigner-like pole, this does not prejudice that such a pole exists in our analysis. We call this treatment of the low energy region *Case A*.

⁵This being a physical process, the imaginary part of each partial wave amplitude must be positive. The authors of Ref. [20] have noted (after the present work was complete) that this favours solution A of LASS [15].

⁶These parameters were provided by W. Dunwoodie and are not the values quoted in the original paper.

While the above *Case A* is largely experimentally motivated, a more theoretically well-founded guide to low energy meson-meson scattering is provided by Chiral Perturbation Theory (χ PT). This makes predictions for near threshold πK scattering that we can input into our analysis. However, the effect of the higher order corrections becomes larger and less immediately predictable as one goes much above threshold. Consequently, we only generate data points based on χ PT within 100 MeV of threshold, with a precision encompassing the range of present calculations [21, 22, 20]. We call this *Case B*. We let the method determine the interpolation between the low energy χ PT results and where LASS data begin. This avoids the need for us to enter into any debate about whether higher order corrections in χ PT are summed better by the Inverse Amplitude method [22, 23] or by explicitly including resonances [21]. Such differences are large at 825 MeV. It is in this sense that we describe our method as “model independent”.

In implementing either *Case A* or *Case B*, we only create a few low energy “data” points so as not overly to prejudice the results. These two alternative sets of “data” are shown in Fig. 6 together with the LASS experimental results below 1 GeV. In both Cases the unphysical cuts are treated as for the model data-set of Sect. 4.

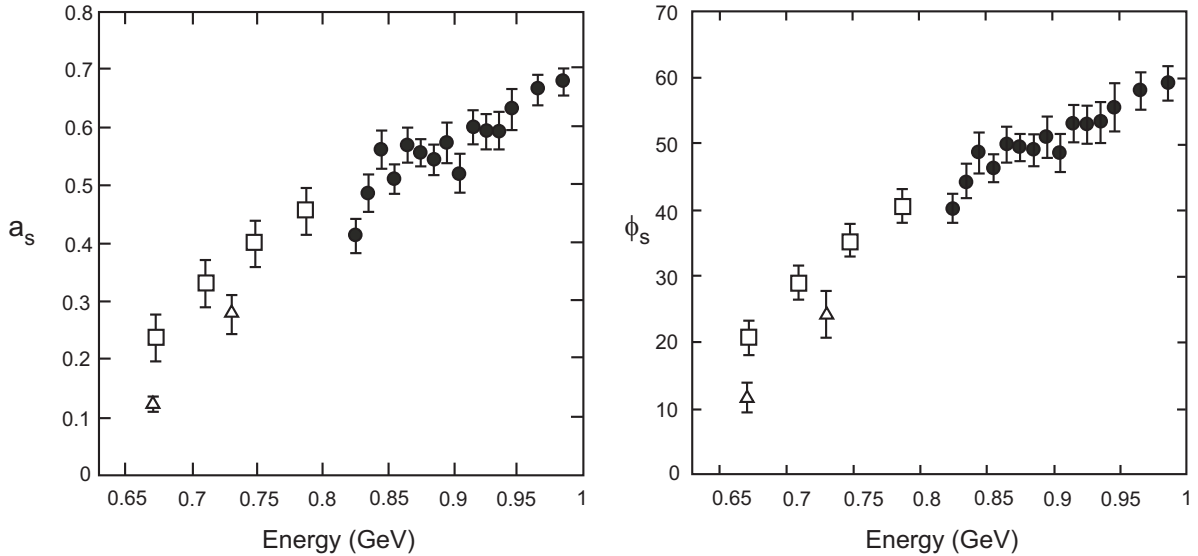


Figure 6: Magnitude, a_s , and phase, ϕ_s (in degrees), of the π^+K^- S -wave below 1 GeV from LASS data (\bullet), contrasting the near threshold fit by the experimental group (\square) with the predictions of χ PT (\triangle).

In Table 3, we present the results of our analysis for the data shown in Fig. 5 and the two extrapolations shown in Fig. 6. The Table shows the pole positions found for the full S -wave data, with full and halved errors on the unphysical points and for the *Case A* and *Case B*

Case	Option	No. of resonances	z_{pole} (r, θ)	$\sqrt{s_{pole}}$ (MeV)	χ^2
A	1	0	—	—	1373
		1	(0.994, 90.07°)	$1433 \pm 149i$	4.7
		2	(0.995, 90.15°) (0.987, 82.02°)	$1432 \pm 148i$ $805 \pm 13i$	1.8
	2	0	—	—	1629
		1	(0.993, 90.06°)	$1423 \pm 157i$	9.0
		2	(0.993, 90.06°) (0.998, 86.98°)	$1423 \pm 154i$ $969 \pm 6i$	8.8
B	1	0	—	—	1340
		1	(0.994, 90.10°)	$1444 \pm 151i$	16.9
		2	(0.994, 90.07°) (0.854, 95.14°)	$1436 \pm 133i$ $609 \pm 238i$	1.0
	2	0	—	—	1694
		1	(0.993, 90.08°)	$1428 \pm 168i$	33.2
		2	(0.994, 90.05°) (0.870, 93.35°)	$1429 \pm 132i$ $645 \pm 260i$	1.0

Table 3: Pole positions and χ^2 's for LASS S -wave data [15] from 0.825 GeV to 2.51 GeV. Cases A and B are explained in the text and shown in Fig. 6.

Option 1: The amplitude in the unphysical region equals the amplitude at threshold, with an error of 5.

Option 2: The amplitude in the unphysical region equals the amplitude at threshold, with an error of 2.5.

continuations to threshold. It is worth pointing out that our method will ‘find’ exactly as many poles as it is asked to. So if we search for two resonances then positions for two resonances will be given no matter how many resonances are present in the data. Resonances that really are present in the data will be stable to changes in unphysical parameters and result in sizeable falls in the χ^2 . Conversely, if the χ^2 does not fall significantly between one and two resonances then we can conclude that the second resonance ‘found’ is not really present and the pole position given is meaningless. Likewise, any resonance found whose pole position changes wildly with variations in parameters not determined explicitly by the experimental πK data used will also be an artifact.

In order to corroborate the results shown in Table 3 the results for the $I = 1/2$ and the shorter S -wave data-sets, using the *Case A* continuation to threshold are shown in Tables 4 and 5. These Tables show a remarkable consistency, as one would hope for effects that are real.

Option	No. of resonances	z_{pole} (r, θ)	$\sqrt{s_{pole}}$ (MeV)	χ^2
1	0	—	—	210
	1	(0.992, 90.22°)	$1467 \pm 224i$	2.1
	2	(0.992, 90.22°) (0.993, 82.14°)	$1464 \pm 221i$ $808 \pm 7i$	1.1
2	0	—	—	367
	1	(0.991, 90.23°)	$1455 \pm 245i$	5.3
	2	(0.991, 90.19°) (0.911, 100.1°)	$1439 \pm 237i$ $503 \pm 238i$	2.4

Table 4: Pole positions and χ^2 's for LASS $I = \frac{1}{2}$ data [15].

Option 1 has unphysical errors set to 5. Option 2 has unphysical errors set to 2.5.

Option	No. of resonances	z_{pole} (r, θ)	$\sqrt{s_{pole}}$ (MeV)	χ^2
1	0	—	—	170
	1	(0.991, 90.03°)	$1471 \pm 242i$	2.2
	2	(0.985, 90.07°) (0.997, 90.08°)	$1422 \pm 553i$ $1457 \pm 80i$	1.9
2	0	—	—	283
	1	(0.991, 90.26°)	$1459 \pm 264i$	5.6
	2	(0.990, 90.23°) (0.886, 101.8°)	$1440 \pm 263i$ $513 \pm 208i$	2.4

Table 5: Pole positions and χ^2 's for the short LASS S -wave data [15].

Option 1 has unphysical errors set to 5. Option 2 has unphysical errors set to 2.5.

As a further check of our results, the same technique was applied to the total S -wave data from an earlier experiment [16]. These data extend closer to threshold, so it is only necessary to create a point at threshold. Barrelet ambiguities lead to four possible partial-wave solutions, which differ only above 1500 MeV, so the choice of solution should not affect our conclusions regarding the κ . We have carried out our analysis using solutions A and B and found the results to be qualitatively similar and so we show only those for solution B. The data are shown below 1 GeV in Fig. 7, which should be compared with the low energy treatment of the LASS data-set (see Fig. 6). This new *Case A* is defined using an effective range formula, see Eq. 20, with $a^{(1/2)} = 2.39 \text{ GeV}^{-1}$ and $a^{(3/2)} = -1.00 \text{ GeV}^{-1}$. No resonance was assumed in this fit, so any lingering doubts that assuming the tail of the $K_0^*(1430)$ in the low energy extrapolation introduces a prejudice is clearly not there in this case. We also consider *Case B* using the scattering length predictions of χ PT, as before. The results for

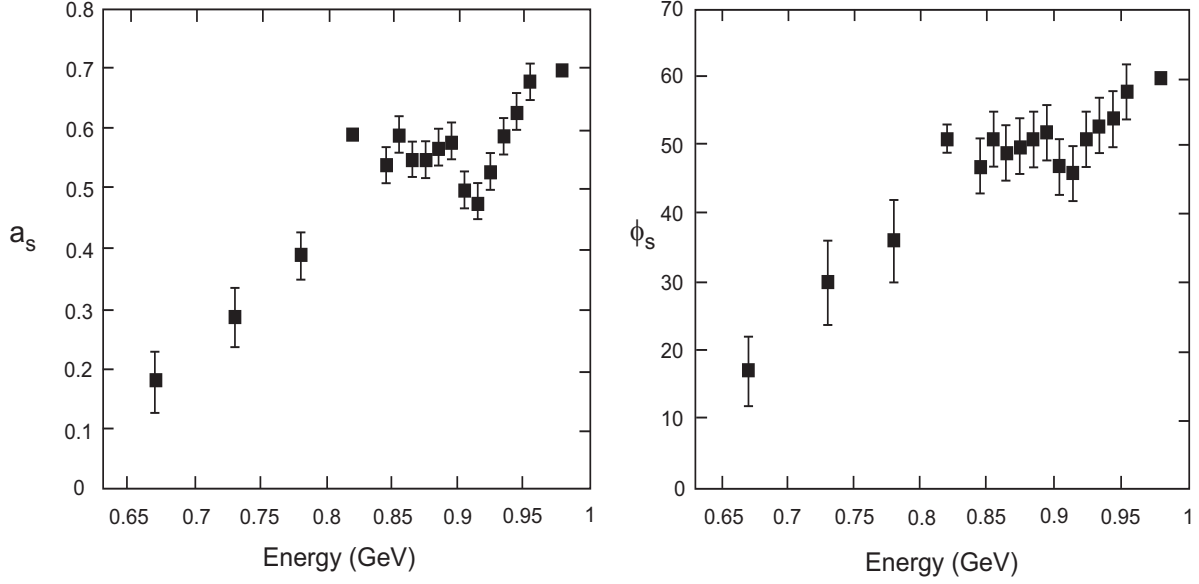


Figure 7: Magnitudes, a_s , and phases, ϕ_s (in degrees) S -wave πK scattering amplitude below 1 GeV from Estabrooks *et al.* [16], to be compared with Fig. 6.

Case	Option	No. of resonances	z_{pole} (r, θ)	$\sqrt{s_{pole}}$ (MeV)	χ^2
A	1	0	—	—	553
		1	(0.991, 90.20°)	$1446 \pm 232i$	16
		2	(0.986, 89.83°) (1.017, 90.46°)	$1277 \pm 231i$ $1344 \pm 444i$	12
	2	0	—	—	812
		1	(0.990, 90.16°)	$1411 \pm 250i$	14
		2	(0.988, 89.92°) (1.01, 90.47°)	$1323 \pm 221i$ $1564 \pm 316i$	14
B	1	0	—	—	551
		1	(0.991, 90.20°)	$1447 \pm 231i$	17
		2	(0.986, 89.84°) (1.015, 90.44°)	$1286 \pm 227i$ $1382 \pm 423i$	14
	2	0	—	—	816
		1	(0.990, 90.16°)	$1411 \pm 253i$	16
		2	(0.991, 89.81°) (1.001, 89.89°)	$1324 \pm 159i$ $1395 \pm 18i$	16

Table 6: Pole positions and χ^2 's for Estabrooks *et al.* [16] S -wave data. The Cases A and B are described in the text.

Option 1 has unphysical errors set to 5. Option 2 has unphysical errors set to 2.5.

the Estabrooks *et al.* data-set [16] are shown in Table 6.

For the real πK experimental results, Tables 3–6 display a consistency in identifying a single resonance which looks very like the $K_0^*(1430)$. The fall in χ^2 in going from no resonance to one resonance is always sizeable, ranging from a factor of 35 to a factor of 290. In contrast when going from one to two resonances, the χ^2 does not always fall by a significant amount. Recall importantly that the present analysis technique is always most sensitive to the lightest resonance and this is clearly the $K_0^*(1430)$. So whilst the $K_0^*(1430)$ is overwhelmingly apparent, a lighter, broad resonance in the LASS range above 825 MeV is not. When using the LASS data and *Case B*, where the low energy behaviour is given by χ PT, there is a sizeable decrease in χ^2 for two resonances, but the very light and broad one is below the experimental ranges studied by both LASS and Estabrooks *et al.*.

Halving the errors in the unphysical region should not greatly affect the pole positions obtained, and from Table 1 we can see that this is indeed the case. From Tables 3–6 we see that for the assumption that there is only one resonance present, then halving the unphysical errors or changing the near threshold continuation, has a small effect. However, when we force the amplitude to have two resonances the effect is much more noticeable. Generally, the resonance which looks like $K_0^*(1430)$ tends to stay in a similar position, but the second one moves around wildly. This is what one would expect if this second resonance is merely an artifact of forcing the method to find two poles that are not really present in the energy range of the data that are being analytically continued into the complex plane.

We mentioned earlier that we would expect the method to be less sensitive to high mass resonances. This is borne out by these results. The LASS group provide strong evidence for a state at 1.95 GeV. With data to 2.51 GeV we would expect to see this state showing up, but the compression of the high energy portion of the amplitude has diluted the effect of the $K_0^*(1950)$ so much that it is not needed to describe the data in the complex z -plane. This is to be expected from our study using model data, described in Sect. 4. The mapping procedure severely limits our ability to find states above 1800 MeV in πK scattering. However, below that, and particularly down towards the lower end of the experimental range, the method is totally reliable and quite unambiguous. Consequently, we have no doubt that

- i. there is a $K_0^*(1430)$,
- ii. there is no $\kappa(900)$,

in experimental πK scattering data.

6 Conclusions

We have here applied a method of analytic continuation in as model independent way as is presently possible to the existing data on π^+K^- scattering between 825 MeV and 2.5 GeV. We find that there is only one scalar resonance between 825 and 1800 MeV, which is readily identified with the $K_0^*(1430)$. Our procedure requires no assumptions about the amplitude being described by Breit-Wigner forms with any particular form of background. It directly counts the number of poles of the S -matrix on the nearby unphysical sheet. This method provides a rigorous test of whether the $\kappa(900)$ exists, and we conclude it does not. This is so whether we use the older Estabrooks *et al.* [16] data or that of the LASS collaboration [15]. Clearly, the question of the existence of a κ of mass and width that does not intrude into the energy range explored by experiment cannot be addressed.

The fact that there is only one strange scalar between 800 and 1800 MeV has implications for quark models that postulate both a $q\bar{q}$ and a $qq\bar{q}\bar{q}$ nonet in this region [5, 24]. Our results of course do not depend on this modelling. However, we cannot refrain from commenting that we believe that other calculations clearly show the scalars are different from other states with underlying $q\bar{q}$ composition. Their decay modes, overwhelmingly to two mesons, mean that the physical hadrons do have a large $qq\bar{q}\bar{q}$ component in their Fock space [11, 12, 13, 25]. Thus for many purposes the scalars below 1800 MeV (particularly those with flavour) do behave like 4-quark states, even though they may well be seeded by single $q\bar{q}$ pairs at the bare level. However, such calculations and speculations are for elsewhere.

We conclude that the data on S -wave πK scattering exhibit just one pair of complex conjugate poles between 0.8 and 1.8 GeV. This means that there is only one resonance present in this channel in the region accessed by the presently highest statistics experiment. This resonance has a mass around 1400 MeV and a width of about 300 MeV. The $\kappa(900)$ does not exist.

Acknowledgements

We are most grateful to Bill Dunwoodie for supplying us with the LASS data and a suitable parametrisation down to threshold. This work was supported in part under the EU-TMR Programme, Contract No. CT98-0169, EuroDAΦNE. One of us (S.N.C.) acknowledges receipt of a studentship from the U.K. EPSRC.

References

- [1] D. E. Groom *et al.*, Eur. Phys. J. **C15** (2000) 1.
- [2] R. Jaffe, Phys. Rev. **D15** (1977) 267;
Phys. Rev. **D15** (1977) 281.
- [3] J. Weinstein and N. Isgur, Phys. Rev. Lett. **48** (1982) 659.
- [4] see, for instance, E. Klempt, Acta. Phys. Polon. **B29** (1998) 3367;
F.E. Close and P.R. Page, Sci. Am. **279** (1998) 52;
C. Michael, hep-ph/9810415, Nucl. Phys. **A655** (1999) 12;
M.R. Pennington, hep-ph/9811276, Proc. of *Workshop on Photon Interactions and the Photon Structure*, Lund, 1998 (ed. G. Jarlskog and T. Sjöstrand) pp. 313-328.
- [5] D. Black, A. H. Fariborz, F. Sannino and J. Schechter, Phys. Rev. **D59** (1999) 074026;
D. Black, A. H. Fariborz and J. Schechter, Phys. Rev. **D61** (2000) 074001.
- [6] R. L. Jaffe, hep-ph/0001123.
- [7] M. D. Scadron, Phys. Rev. **D26** (1982) 239.
- [8] R. Delbourgo and M. D. Scadron, Int. J. Mod. Phys. **A13** (1998) 657.
- [9] D. Black, A. H. Fariborz, F. Sannino and J. Schechter, Phys. Rev. **D58** (1998) 054012.
- [10] S. Ishida, M. Ishida, T. Ishida, K. Takamatsu and T. Tsuru, Prog. Theor. Phys. **98** (1997) 621.
- [11] E. Van Beveren, T. A. Rijken, K. Metzger, C. Dullemond, G. Rupp and J. E. Ribeiro, Z. Phys. **C30** (1986) 615.
- [12] J. A. Oller and E. Oset, Phys. Rev. **D60** (1999) 074023.
- [13] N. A. Tornqvist, Z. Phys. **C68** (1995) 647.
- [14] A. V. Anisovich and A. V. Sarantsev, Phys. Lett. **B413** (1997) 137.
- [15] D. Aston *et al.* (LASS Collaboration), Nucl. Phys. **B296** (1988) 493.
- [16] P. Estabrooks, R. K. Carnegie, A. D. Martin, W. M. Dunwoodie, T. A. Lasinski and D. W. Leith, Nucl. Phys. **B133** (1978) 490.

- [17] A. Nogová, J. Pišút, and P. Prešnajder, Nucl. Phys. **B61**, (1973) 438;
A. Nogová, J. Pišút, Nucl. Phys. **B61**, (1973) 445.
- [18] See e.g. J. T. Taylor *Scattering Theory* John Wiley & Sons (1972);
R. J. Eden, P. V. Landshoff, D. I. Olive and J. C. Polkinghorne *The Analytic S-Matrix*
CUP (1966).
- [19] P. Estabrooks, Phys. Rev. **D19** (1979) 2678.
- [20] M. Jamin, J. A. Oller and A. Pich, hep-ph/0006045.
- [21] V. Bernard, N. Kaiser and U. G. Meissner, Nucl. Phys. **B357** (1991) 129;
V. Bernard, N. Kaiser and U. G. Meissner, Nucl. Phys. **B364** (1991) 283.
- [22] A. Dobado and J. R. Pelaez, Phys. Rev. **D47** (1993) 4883.
- [23] J. A. Oller, E. Oset and J. R. Peláez, Phys. Rev. Lett. **80** (1998) 3452;
J. A. Oller, E. Oset and J. R. Peláez, Phys. Rev. **D59** (1999) 074001;
Erratum-ibid. **D60** (1999) 099906
- [24] M. Alford and R. L. Jaffe, hep-lat/0001023.
- [25] M. Boglione and M. R. Pennington, hep-ph/9703257, Phys. Rev. Lett. **79** (1997) 1998.